Design and construction of catenary-ruled surfaces

Zhi Li [a], Ting-Uei Lee [a], Nico Pietroni [b], Roland Snooks [c], Yi Min Xie [a,*]

[a] Centre for Innovative Structures and Materials, School of Engineering, RMIT University, Melbourne, 3001, Australia
[b] Faculty of Engineering and Information Technology, School of Computer Science, University of Technology Sydney, Sydney, 2007, Australia
[c] RMIT Architecture – Tectonic Formation Lab, School of Architecture and Urban Design, RMIT University, Melbourne, 3001, Australia

ARTICLE INFO

ABSTRACT

The past two decades have witnessed an increasing adoption of double-curved surfaces in architectural design and building construction. However, their shape complexity has brought a great challenge in design and construction, typically leading to high modeling and construction costs. In this study, a new geometry family, termed catenary-ruled surface, is proposed. They can be conveniently created using catenary rulings based on the transformation of line rulings, thereby offering new possibilities for designing a wide variety of architectural forms. Moreover, this paper uses a physical model to demonstrate that a specific group of catenary-ruled surfaces can be effectively and inexpensively constructed using a proposed string actuation system. This is achieved by using a series of foldable arches to form the target surface, with their folding motion controlled by simply pulling external strings. The constructed structure with catenary rulings can act as an efficient structural system that is predominantly under pure compression.

1. Introduction

Curved surfaces are striking 3D forms typically with no part that is a plane surface, meaning both of their principal curvatures cannot be zero simultaneously. In recent years, curved surfaces have been increasingly adopted in architectural designs, such as pavilions [1–3], bridges [4,5], and roofs [6,7], due to the development of computer-aided design technologies and the increasing sophistication of digital fabrication [8–10]. However, the use of curvatures has brought a great challenge in design and construction, which may lead to high modeling and construction costs. Due to this, recent research effort has been devoted to modeling techniques [11–18], and construction methodologies [19–22] of curved surfaces, aiming to achieve simple and cost-effective solutions.

Among many curved surface modeling techniques, the line-ruled surface design technique is a popular strategy, as diverse curved surfaces can be simply and effectively created by utilizing the continuous motion of a straight ruling [23–26]. Recently, a new type of ruled surface composed of elastica rulings, the elastica-ruled surface, has been developed based on the transformation of line-ruled surfaces [27–30]. Elastica curves are minimum bending energy configurations of a straight, slender beam, as shown in Fig. 1. Hence, elastica-ruled surfaces have been demonstrated to have high suitability for practical applications that consider elastic bending behavior. There is a vast potential to utilize other curves to create curve-ruled surfaces, which may lead to interesting and useful performative characteristics.

Catenary curves also have attractive mechanical properties. They are 2D funicular geometries representing a cable hanging under its self-weight in a uniform gravitational field [31,32]. Compared with elastic curves, the shapes of catenary curves have a larger vertical deformation under the same curve length and boundary conditions, as shown in Fig. 1(a). Moreover, Fig. 1(b) shows the shape of inverse catenary curves, which can be used to create an efficient structural form—compression structures [9]. Such structures carry compression load only with no bending or tension loads due to a large self-weight compared to the applied load [33–35]. Thus, architects prefer to use catenary curves to design stable curved structures in large-scale architectural projects [36]. For example, the famous architect, Antoni Gaudí, used catenary curves to design the compression structures of the Sagrada Família [37–39]. Therefore, catenary curves have a huge potential to be used as curved rulings to create double-curved surfaces for large-scale applications.

However, the large-scale construction of curve-ruled surfaces is a tricky problem due to their double-curved shapes. Existing construction techniques are often costly and labor intensive, as they require the target surface to be divided into smaller panels to satisfy construction constraints (e.g., the size of panels must be designed considering manufacturing and transportation methods) [40]. It should be noted that using smaller panels would lead to numerous construction challenges. For example, positioning and aligning (i.e., assembling) the panels to
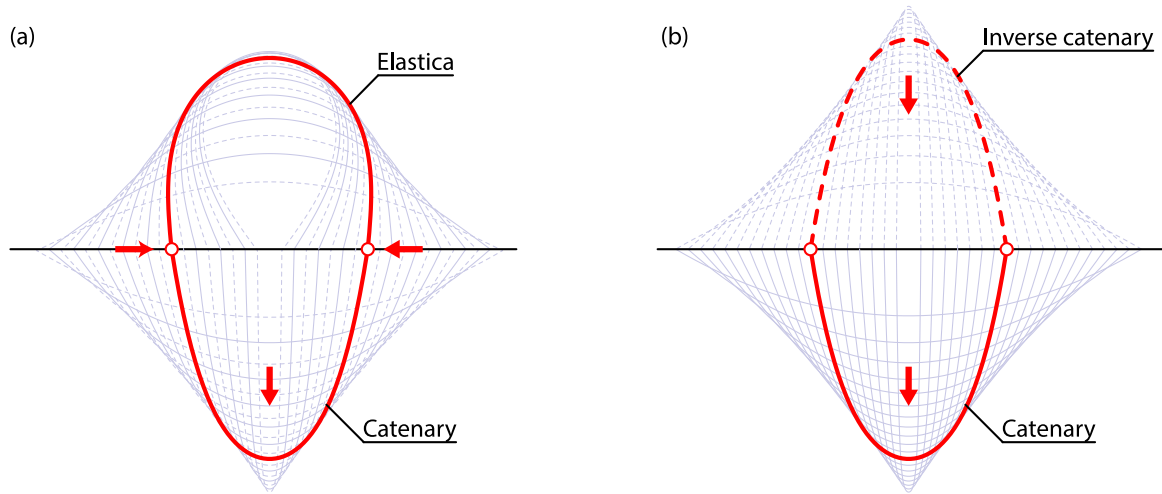
Fig. 1. Comparison of curve shapes under the same curve length and boundary conditions: (a) elastic curves and catenary curves; (b) catenary curves and their inverse curves.

their target locations are extremely tedious and time-consuming tasks. Besides, the assembling process may require a significant amount of formwork to temporarily support the panels during construction [1,19, 41,42], thereby generating additional material waste, fabrication costs, and workload.

Suppose panels of a curved surface are connected with a hinge mechanism. In that case, the *string actuation system* can be employed to automate the assembling process through folding [43], thereby significantly reducing construction costs. Specifically, connected panels can be considered a mechanical mechanism, and the folding motion can be controlled by utilizing the movement of pulled external strings. Such a construction method has been successfully employed in large-scale constructions, including timber arches [44] and concrete bridges [45, 46]. However, the actuated curved surfaces are often simple; they typically are simple arch forms with the design surface possessing a zero Gaussian curvature. The string actuation system can also be used to construct double-curved surfaces. This is achieved by using the gridshell system [47–50]. However, the actuated form typically is not a continuous surface due to the use of bent, slender elements. Extending the string actuation system to the construction of continuously double-curved surfaces is an ongoing challenge and remains under-explored.

This paper proposes a new type of curve-ruled surfaces, termed *catenary-ruled surfaces*, which can be conveniently designed using catenary rulings and inexpensively constructed using the string actuation system to achieve double-curved surfaces.

The main contributions of this paper are summarized as follows:

- A new type of ruled surface composed of catenary-curved rulings is proposed. Such surfaces can be fully controlled by four design parameters, offering new possibilities to create complex surfaces parametrically.
- The proposed surfaces can be used to create compression-dominant structures, with each curved ruling corresponding to a catenary arch for bearing gravity loads, thereby making the most effective use of the catenary property.
- A novel string actuation system is developed to reduce the on-site construction effort of the proposed surface. This is achieved by first dividing the catenary-ruled surface into self-supporting arches consisting of hexagonal panels and then assembling each arch by actuating strings to realize the proposed surface.
- The experiments show that the constructed structures are stable, and the construction method includes self-correction mechanisms during the assembly process, greatly reducing costs and labor resources, as demonstrated in the accompanying video.

The remainder of the paper is organized as follows: Section 2 describes the geometric modeling method. Section 3 explains the details of the proposed string actuation system. Section 4 shows an experimental analysis, followed by the conclusion highlighting the key features of catenary-ruled surfaces in Section 5.

2. Creation of catenary-ruled surfaces

2.1. Catenary curves

For a cable, fixing its two ends and making it drop naturally can easily obtain a catenary curve in the real world, as shown in Fig. 2(a). To more accurately describe this curve, previous research has developed analytical solutions to draw an ideal catenary curve [31,51], briefly summarized here as follows.

As shown in Fig. 2(b), a catenary curve created between points $A(x_1, y_1)$ and $B(x_2, y_2)$ has four design parameters: the arc length of the curve, L, the horizontal opening distance, $b = |x_2 - x_1|$, the vertical distance between curve ends, $h = |y_2 - y_1|$, and the prescribed gravity direction, $\vec{G}$.

The shape of a catenary curve can be described using a hyperbolic cosine function to determine the (x, y) Cartesian coordinates:

$$y = a \cosh(\frac{x + p}{a}) + q \tag{1}$$

where y is the unknown; x ranges from x_1 to x_2; a is a positive parameter related to the overall shape of the curve, and increasing a can improve the width-to-height ratio; p and q are the horizontal and vertical shifts, respectively. Parameters a, p, and q can be determined using curve design parameters L, b, and h, as shown in Eqs. (2)–(4). Note that, for ease of calculation, Eqs. (2)–(4) assume a fixed $\vec{G}$ to be $(0, -1)$. Designing a catenary curve with a different $\vec{G}$ requires the curve to be translated and rotated to match the assumed $\vec{G}$.

The relationship between parameters a, L, b, and h is given as:

$$\sqrt{L^2 - h^2} = 2a \sinh(\frac{b}{2a}) \tag{2}$$

Eq. (2) with specified L, b, and h can be solved using the Newton's method [52] to obtain a.

Once a is obtained, p and q can be calculated:

$$p = \frac{a \ln(\frac{L+h}{L-h}) - x_1 - x_2}{2} \tag{3}$$

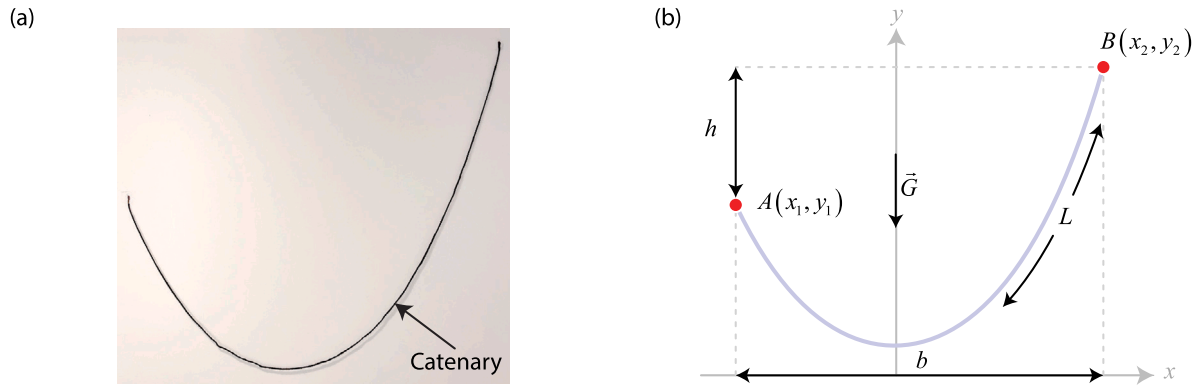$$q = \frac{y_1 + y_2 - L \coth(\frac{b}{2a})}{2} \tag{4}$$

Fig. 2. Catenary curve. (a) Photo of a hanging cable, (b) catenary curve design parameters.
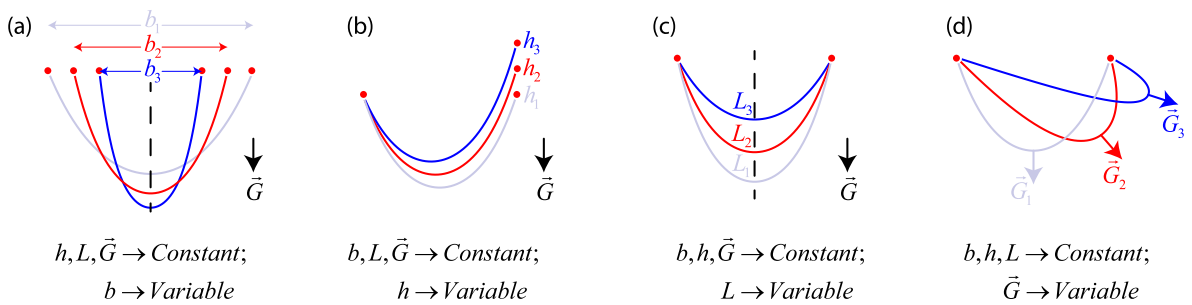

Fig. 3. Controlling the shape of a catenary curve using a variable. (a) Horizontal opening distance, b, (b) vertical distance between curve ends, h, (c) arc length of the curve, L, and (d) gravity direction, $\vec{G}$.

Together, substituting a, p, and q into Eq. (1) gives an explicit mathematical description of a unique catenary curve. Specifying a range for x, $x_1 < x < x_2$, in Eq. (1) gives the y-coordinates, thereby obtaining (x, y) coordinates to construct the catenary curve.

It should be noted that the shape of a catenary curve can be fully controlled by its four design parameters, L, b, h, and $\vec{G}$, demonstrated more clearly in Fig. 3. For example, setting b to be the variable with other design parameters fixed can simulate the shape of a hanging cable supported under different opening distances, as shown in Fig. 3(a); setting h to be the variable can simulate the hanging cable with one end moved to different heights, as shown in Fig. 3(b); setting L to be the variable can simulate cables of different lengths hung under the same boundary condition, as shown in Fig. 3(c); and setting $\vec{G}$ to be the variable can simulate the cable hung in different gravitational fields, as shown in Fig. 3(d).

2.2. Transformation of line-ruled surfaces

A series of catenary curves can be used as curved rulings to create a new type of curve-ruled surfaces, termed 'catenary-ruled surfaces'. Specifically, catenary-ruled surfaces are created based on the transformation of input line-ruled surfaces (see Fig. 4), similar to the transformation method described in [27]. The transformation first requires a line-ruled surface to be predetermined using directrices and straight rulings, as shown in Fig. 4(a). The shape and position of the two directrices determine b and h of each curved ruling under an assumed gravitational vector $\vec{G}$. The parameter L, determining the arc length of a catenary curve, completes the definition of each catenary ruling, as shown in Fig. 4(b). Finally, employing the two directrices as guiding rails and the catenary rulings as sectional curves can create a catenary-ruled surface. This is achieved by seamlessly sweeping the catenary rulings along the directrices, as shown in Fig. 4(c) [8,53]. Note that if $L = b$, the transformation result is a line-ruled surface. Hence, line-ruled surfaces can be understood as extreme catenary-ruled surfaces.

Using the proposed transformation method, a wide variety of double-curved catenary-ruled surfaces can be simply, parametrically, and conveniently created, with examples shown in Fig. 5. It should be noted that if the two directrices are of different shapes, the lengths of line rulings are different, resulting in a catenary-ruled surface with a varying b, as shown in Fig. 5(a). If the directrices are different space curves, the line-rulings are inclined continuously, resulting in a catenary-ruled surface with a varying h, as shown in Fig. 5(b). If the directrices are of the same shape, the line-ruled surface is developable with a zero Gaussian curvature, and a varying L ($> b$) must be specified to create a double-curved catenary-ruled surface, as shown in Fig. 5(c). The shape of a catenary-ruled surface can be further modified using a varying $\vec{G}$, as shown in Fig. 5(d).

2.3. Potential structural advantages

Catenary-ruled surfaces naturally inherit the mechanical properties of their sectional catenary curves. As mentioned in Section 1, an inverse catenary curve is the most efficient compression structure. Inverse catenary-ruled surfaces can also be considered compression-dominant structures, as each sectional curve of a surface can carry mainly the compression load generated from the self-weight [34,54]. According to [9], compression-dominant structures have efficient material utilization, as many construction materials, such as concrete and stone, can withstand greater forces under compression than under tension or bending. Moreover, structures under compression are more stable and durable because the fatigue and damage accumulation in materials are slower under compression, contributing to a longer lifespan of the structure. Based on these advantages, utilizing inverse catenary-ruled surfaces can enhance structural efficiency and stability, resulting in more sustainable structural designs.
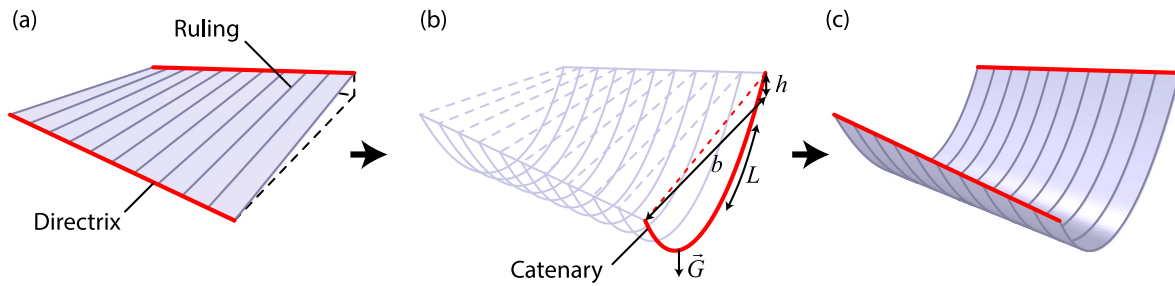
Fig. 4. Creation of a catenary-ruled surface. (a) Lined-ruled surface, (b) catenary curves on line rulings, (c) continuous surface obtained from catenary rulings.
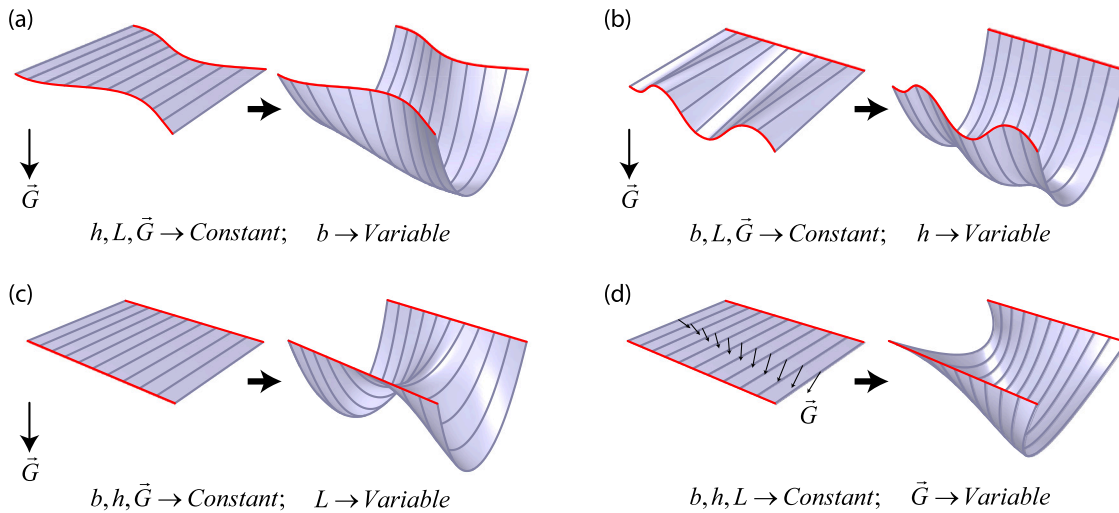

Fig. 5. Creating catenary-ruled surfaces using a variable. (a) Horizontal opening distance, b, (b) vertical distance between curve ends, h, (c) arc length of the curve, L, and (d) gravity direction, $\vec{G}$.

2.4. Conceptual design examples

The proposed catenary-ruled surfaces offer new design possibilities to create elegant and well-defined architectural forms. Three conceptual design examples, including a tunnel, roof, and chair, are shown in Figs. 6(a)–(c), respectively.

The tunnel and roof are designed using the shape of 'inverse catenary-ruled surfaces'. Specifically, the curved surfaces possess 'inverse catenary rulings', meaning the catenary curves are designed to have a fixed $\vec{G} = (0, 0, 1)$ (i.e., opposite to the gravity direction). As mentioned in Section 2.3, such generated forms are considered compression-dominant structures, which have a high level of material utilization, stability, and durability.

The chair is designed to possess the catenary rulings popping outward, achieved by allowing a varying $\vec{G}$. It should be noted that the shape of the chair may be further modified by changing parameters, L, b, h, and/or $\vec{G}$. In doing so, diverse novel designs sharing the same 'base' line-ruled surface can be generated, thereby offering new design possibilities for creating elegant architectural forms. For example, the sitting area of the chair may be enlarged using a larger L, and the positions of armrests can be adjusted by modifying $\vec{G}$.

3. Constructing catenary-ruled surfaces

3.1. Proposed string actuation system

Another contribution of this research is the development of a novel string actuation system that can simply and rapidly realize inverse catenary-ruled surfaces. To demonstrate the concept of the new construction method, the tunnel design shown in Fig. 6(a) is selected to be the tested geometry, used in Sections 3–4. The tunnel design has both

directrices specified on the same base plane, resulting in all inverse catenary rulings being symmetrical to reduce the shape complexity. Moreover, this tunnel form can be subdivided into a series of simple arches, but with the design surfaces possessing a double curvature. Due to the use of catenary rulings, each component arch can be considered a catenary arch, corresponding to a compression structure that can stand under its own weight. Besides, each arch is segmented into smaller panels and connected to form a mechanical mechanism so that the folding motion can be controlled by the movements of pulled external strings.

To achieve the proposed string actuation system, the given catenary-ruled surface must be further modified. This includes converting the surface geometry into solid curved panels (see Section 3.2) and imparting them with connection details (see Section 3.3). Connected panels can be lifted and automatically assembled into a series of target catenary arches, achieved simply by pulling external strings in the vertical direction, with details described in Section 3.4.

3.2. Creation of solid curved panels

The proposed system requires the division of catenary-ruled surfaces into self-supporting sub-structures that can be assembled individually by lifting and placing, introduced in Section 3.4. Since one direction of the catenary-ruled surface is the catenary rulings, and the other direction is along the user-defined free-form directrices, the best-dividing strategy is to perform subdividing in a direction parallel to the catenary rulings. This approach takes advantage of the compression-dominant properties of the catenary, while the neighboring catenary arches serve as support to resist minor inclinations from the direction of free-form directrices.
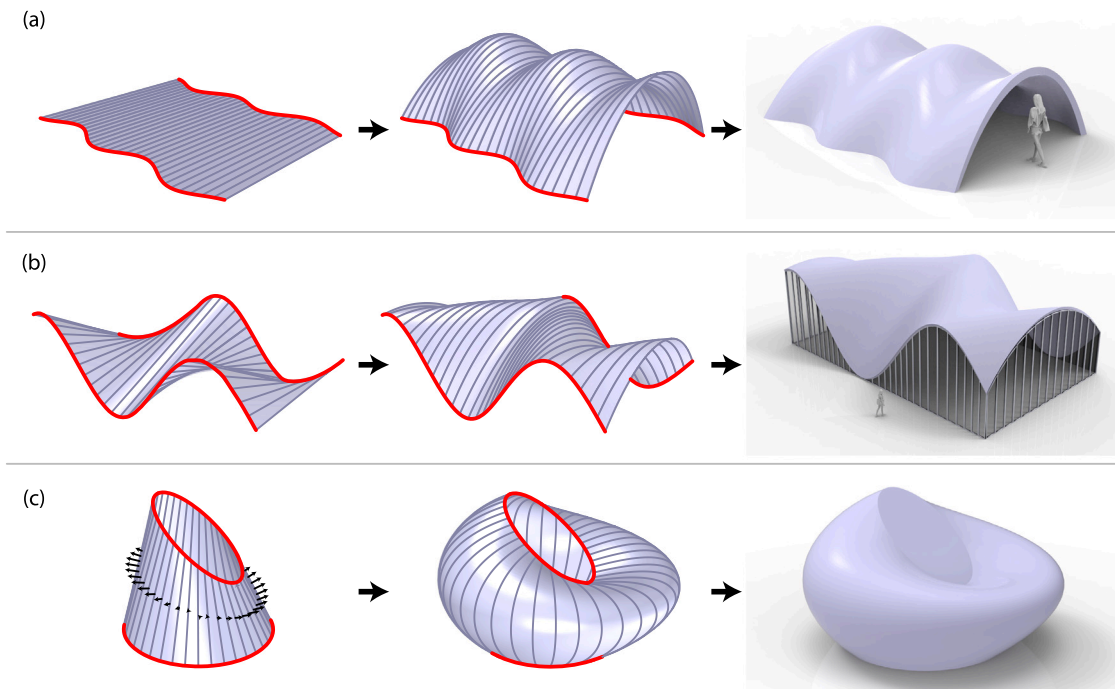
Fig. 6. Potential practical applications of catenary-ruled surfaces. (a) Tunnel, (b) roof, and (c) chair.
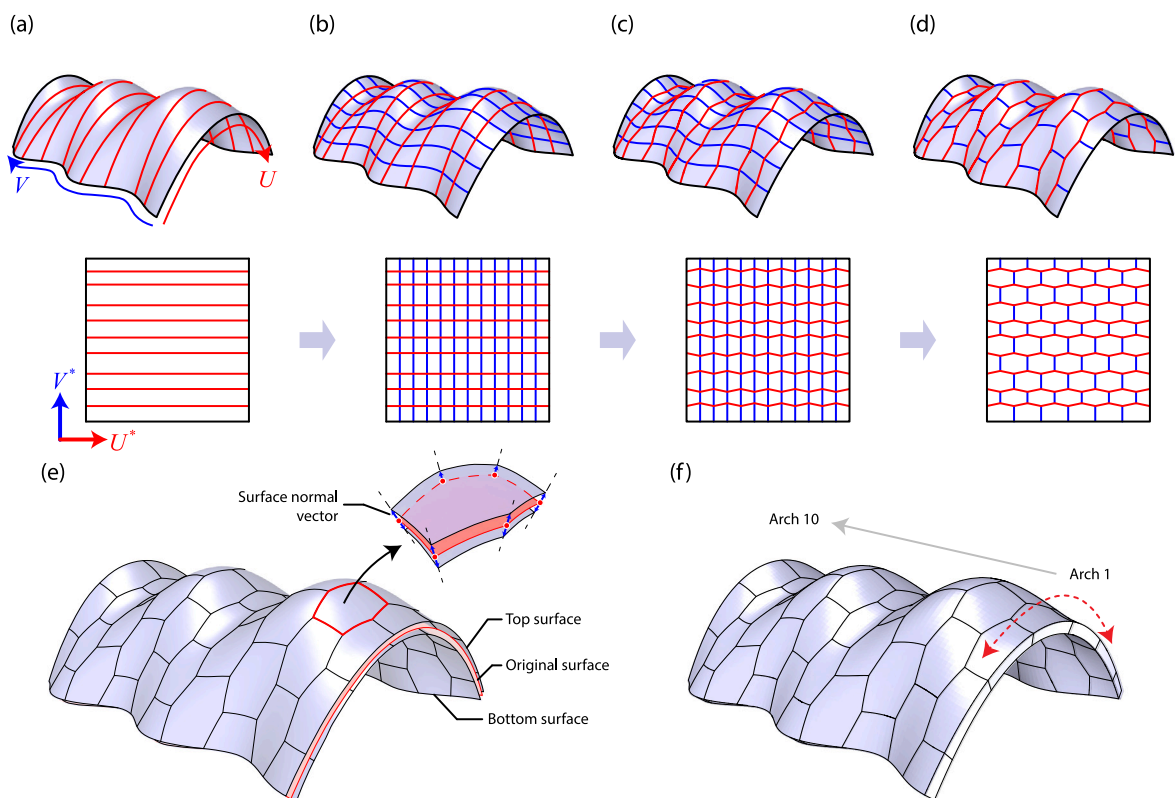

Fig. 7. Creating solid hexagonal curved panels. (a) The divided catenary arches are mapped onto a square parametric domain, (b)–(d) creating curved hexagonal panels using the proposed penalization method. The 2D graphs are the parametric domains. (e) offsetting the hexagonal panels on both sides; (f) connecting the offset faces gives solid panels. (For interpretation of the references to color in this figure legend, the reader is referred to the web version of this article.)

Using the aforementioned idea, the 'tunnel-like' catenary-ruled surface, as shown in Fig. 7(a), is first subdivided into ten catenary arches. It should be noted that the subdivision is performed considering 'curvature variations', resulting in arches of different widths. Specifically, the subdivision gives a prescribed number of arches while ensuring the catenary rulings in each arch are of similar sizes and shapes. This process aims to create 'near-linear-tunnel-like' arches so that each can have a structural performance similar to an inverse catenary curve, that is, stable under its self-weight [34], validated later in Section 4.2. Note that the subdivision is achieved using the proposed *splitting algorithm* with details summarized in Appendix A.

The simple arches shown in Fig. 7(a) are further modified to create arches composed of curved hexagonal panels, as shown in Figs. 7(b)–(d). Using hexagonal panels gives zig-zag boundaries between adjacent arches to introduce an interlock mechanism, which can improve the positioning accuracy when putting actuated arches together. The panelization process, seen in Figs. 7(a)–(d), is achieved using the surface parameterization method [55–57]. To clearly illustrate this method, the directions along the catenary rulings and directrices are defined as U and V directions, respectively. Consequently, every point on the catenary-ruled surface can be represented by parametric coordinates, (u, v). The surface parameterization method can project all points onto a unit square by normalizing their (u, v), referred to as the parametric domain. Therefore, an invertible mapping correspondence between the original three-dimensional surface and the two-dimensional parametric domain is established (see sub-figures of Figs. 7(a)–(d)), enabling users to conveniently obtain desired local shapes on a 3D configuration based on 2D geometric operations. More significantly, the size of panels can be simply controlled using this method to satisfy construction constraints [19,40], including manufacturing and transportation constraints. The detailed steps of the panelization process are shown as follows:

- Step 1, (Fig. 7(a)): Map the divided catenary arches onto a square parametric domain, aligning the U and V directions of the catenary-ruled surface. Label the corresponding mapped directions on the parametric domain as U^* and V^*.
- Step 2, (Fig. 7(b)): Equidistantly divide the parametric domain along the U^* direction. The splitting lines (blue lines) intersect the arch boundaries (red lines) to form rectangular panels.
- Step 3, (Fig. 7(c)): Adjacent two rectangles are converted into two symmetric isosceles trapezoids along their shared edges.
- Step 4, (Fig. 7(d)): Remove the shared edges of adjacent trapezoids to create hexagons.
- Step 5, (Fig. 7(e)): Map the hexagons back onto the original catenary-ruled surface. Offset the hexagons along both the positive and negative normal vector direction of the surface to create a top surface and a bottom surface [8,58].
- Step 6, (Fig. 7(f)): Connect the boundaries of the hexagons on the top and bottom surfaces to generate solid hexagonal panels.

3.3. Connection details

In the proposed string action system, solid hexagonal panels in each arch are connected, with connection details shown in Fig. 8. It can be seen that each panel includes six rings, where two rings are in the middle region (named *middle rings*), and the remaining rings are located around the boundary edges (named *boundary rings*). Moreover, the panels are connected with two types of strings, including *actuation* (red) and *connection* (blue) strings. The actuation string is put through the middle rings of all panels in a global closed-form, as shown in Fig. 9. Hence, pulling the actuation string can force the gaps between panels to be closed, thereby achieving the target catenary arch. The connection strings are put through the boundary rings locally between the panels. They provide connectivity and are also capable of preventing panels from rotating around the actuation string during the folding motion.
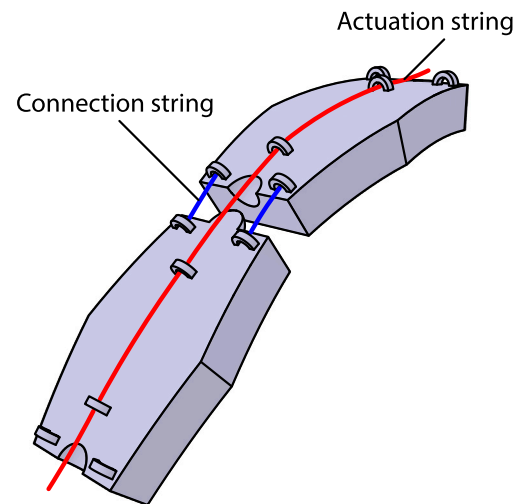

Fig. 8. Connection details between solid hexagonal panels. (For interpretation of the references to color in this figure legend, the reader is referred to the web version of this article.)

It should be noted that the catenary arches are double-curved. Hence, they cannot form straight and flat strips when lying on the ground. Besides, arranging the panels on the ground can be challenging, as the relaxed positions of double-curved panels can introduce a 'height difference', resulting in the edges of panels may not be perfectly aligned. To this end, hemispherical male and female joints are employed between panels (see Fig. 9), which provide instruction to position panels on the ground and form a hinge mechanism when the panels contact each other to guide the folding motion.

3.4. Automatic assembly

The proposed string actuation system can automatically assemble the hexagonal panels to their target locations to form catenary arches, as shown in Fig. 9. It can be understood that the assembly process includes four stages, as shown in Figs. 9(a)–(d), respectively, with details described as follows.

Stage 1 is the preparation phase, where panels are laid on the ground (instructed by the joints) and connected using actuation and connection strings. Stage 2 requires the actuation string to be pulled vertically at the mid-location. In doing so, the gaps between panels can be gradually closed, determined by the lifting height. Note that the target catenary arch is achieved when it is hung in the air. Stage 3 places the assembled arch in its design location. Stage 4 removes the actuation string. It is worth pointing out that stage 4 is optional. Although the arch is stable under its self-weight without the actuation string, the actuation strings may be post-tensioned to enhance the structural performance. However, this will not be closely studied in the present paper. Finally, repeating stages 1–4 for all arches completes the construction of a continuous catenary-ruled structure.

4. Experimental analysis

4.1. Method

To examine the effectiveness of the proposed string actuation system, two experiments were conducted. They were the *lifting* and *placing* tests, corresponding to the processes of stages 1–2 and 3–4 described in Section 3.3, respectively.

The lifting test was performed using a simple catenary arch, as shown in Fig. 10(a). The arch was made up of six 12 mm thick 3D-printed solid hexagonal panels connected using a cotton string and cable ties to represent actuation and connection strings, respectively.
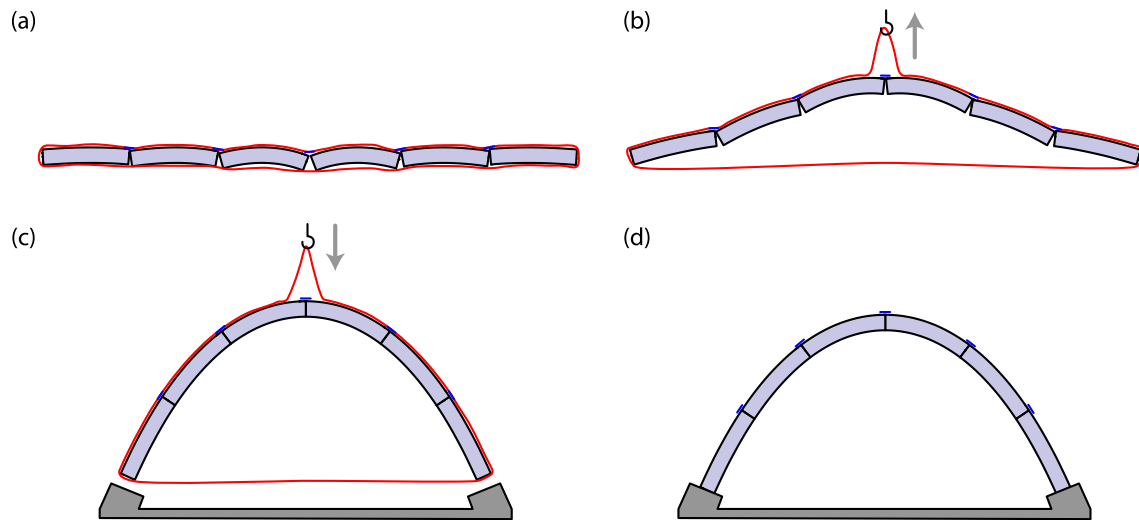
Fig. 9. The proposed string actuation system includes four stages to automatically assemble the panels to a catenary arch. (a) Stage 1 is the preparation phase, (b) stage 2 lifts the design components by pulling the actuation string, (c) stage 3 places the assembled arch in its design location, (d) stage 4 removes the actuation string. (For interpretation of the references to color in this figure legend, the reader is referred to the web version of this article.)
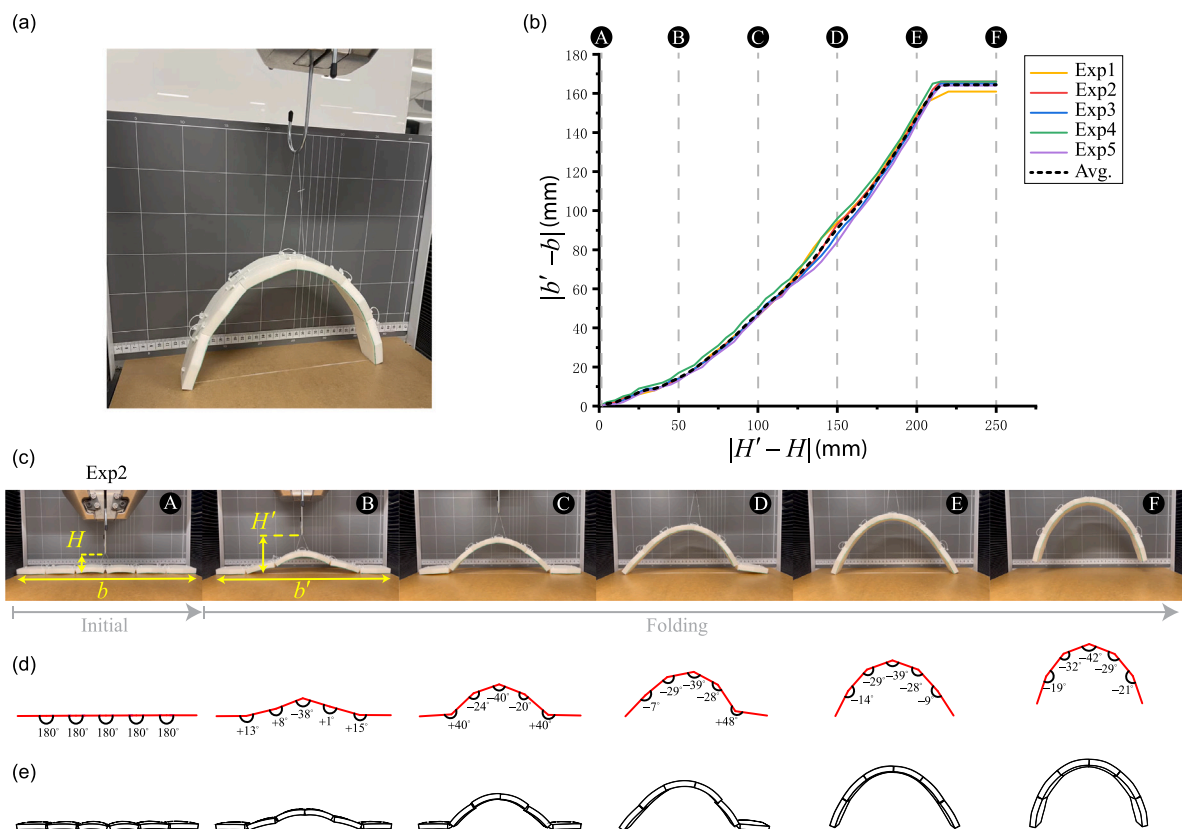

Fig. 10. Lifting test. (a) Experimental setup, (b) historical data of horizontal and vertical changes, (c) photos of Exp2, (d) bar-and-hinge model created based on measured angles, and (e) 3D simulation achieved using the bar-and-hinge model.

The unactuated arch at stage 1 had an approximate size of 414 mm (width) × 21 mm (height) × 45 mm (depth), and the target arch at stage 2 had an approximate 5size of 286 mm (width) × 138 mm (height) × 45 mm (depth). The transformation of stages 1–2 was achieved using an Instron Universal Testing machine, with a displacement control set to be 5 mm/s. The maximum vertical displacement was set as 250 mm so that the actuated arch with a target shape at stage 2 was hung in the air. The lifting test aimed to understand the folding behavior of the catenary arch based on the observations of measured vertical ($|H' - H|$) and horizontal ($|b' - b|$) changes in the entire system, as

shown in Figs. 10(b)–(c). Note that H and H' were the heights measured from the ground to the endpoint of the pulled actuation string at the initial and folding states, respectively; b and b' were the initial and actuated arch opening distances, respectively.

The placing test was performed by manually and sequentially putting together all ten actuated arches of the tunnel design (see Fig. 7(e)) to form the prescribed catenary-ruled surface, as shown in Fig. 11. The tunnel had an approximate size of 339 mm (width) × 142 mm (height) × 403 mm (depth). It was made up of ten catenary arches, each composed of six or eight 12 mm thick 3D-printed solid
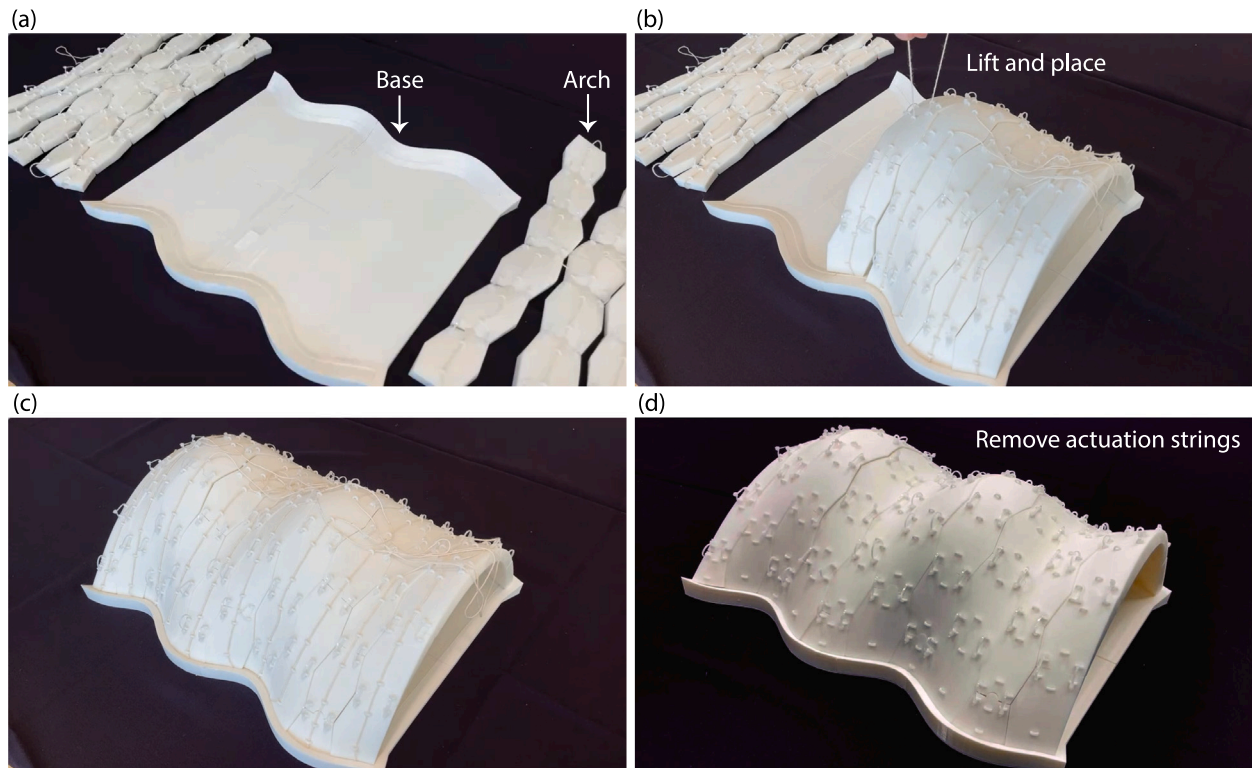
Fig. 11. Placing test. (a) Components preparation, (b) demonstration of the 'lift and place' process, (c) all actuated arches are in their target locations to form the tunnel, and (d) the stable tunnel with removed actuation strings.

hexagonal panels, resulting in a total of 65 panels (see Fig. 7(d)). The connection materials and details were the same as the simple arch used in the lifting test. Moreover, a base was 3D-printed to guide the positioning process, as shown in Figs. 11(a)–(b). Once all arches were in their target positions, the actuation strings were removed. The aim of the placing test was to explore possible difficulties of the proposed string actuation system in large-scale constructions reported based on the observations of the present prototype.

4.2. Results

4.2.1. Lifting test

The lifting test was repeated five times, with results summarized in Fig. 10(b). It can be clearly seen that the five historical data trends are similar (see Exp1–Exp5), representing that a consistent folding behavior has been achieved. It is worth pointing out that the folding motion was complex, demonstrated more clearly using the photos of Exp2 (see Fig. 10(c)). In detail, the four middle panels were first lifted while the two end panels gradually approached each other on the ground (see steps A–C). Later, one side of the end panel was lifted, and the other end panel remained on the ground (see step D). Finally, all panels were lifted, resulting in the target catenary arch forming in the air (see steps E–F). Together, as shown in Fig. 10(b), a non-linear trend plus a curve plateau have been achieved, corresponding to steps A–D and E–F, respectively. It can be noted that data curves at step D had the biggest variation, as the end panels may take off on either side or simultaneously. Moreover, the formation of the curve plateau seen in steps E–F was due to the achievement of the target catenary arch, meaning the horizontal displacement could not be further changed while the arch was hung in the air.

Based on the observations of the lifting tests, it was found that one side of the strip was raised prior to the other during the lifting process. This can be attributed to two factors. Primarily, achieving a perfect lifting process along the centroid of a strip is practically difficult, leading to asymmetrical pulling forces. Furthermore, although

the strips are lifted at a consistent speed in the lifting tests, small vibrations occur due to collisions between components. However, even if the initiation in step D is asymmetric, all panels can be assembled to their target locations to achieve the designed catenary arch later in step F, corresponding to a self-correction mechanism. This has confirmed the effectiveness of the proposed string actuation system, where catenary arches can be simply and accurately achieved utilizing the self-correction mechanism, thereby leading to inexpensive constructions. It should be noted that the self-correction mechanism was attributed to the use of a closed-form actuation string. Specifically, the pulled actuation string was gradually tightened during lifting, thus forcing the gaps between panels to be closed and correcting the assembly errors. Note that the distance from the top surface of the catenary arch to the endpoint of the pulled actuation string was increased during lifting.

The folding behavior can be further studied using the angle data between adjacent panels. This may be achieved using a bar-and-hinge model with measured angles, as shown in Fig. 10(d). Having a bar-and-hinge model allows the lifting test to be reproduced in a computational environment through mapping, resulting in a 3D simulation possessing solid curved panels, as shown in Fig. 10(e). Such an accurate 3D simulation, considering the folding motion and the geometries, allows engineers to perform reliable structural analysis. However, this is not the primary interest of this study; our future study will include examining the structural performance of folding catenary arches.

4.2.2. Placing test

As shown in Figs. 11(a)–(c), the catenary arches were sequentially actuated and placed at their target locations on the base. Later, all actuation strings were removed to form a stable tunnel, as shown in Fig. 11(d). The entire process took approximately three minutes, and the time was mainly spent on manual operations of correcting the locations of arches and removing the actuation strings. It should be noted that the 'lift and place' process of all ten arches took less than a minute, which was achieved by controlling the movement of

a single point on each actuation string. This has confirmed that the proposed string actuation system was simple, rapid, and labor-saving. Besides, the arches were easily aligned due to the use of zig-zag boundaries. More significantly, temporary supports were not needed during construction, thus avoiding additional material waste and workload. Together, it can be concluded that the proposed string actuation system is an effective strategy to achieve double-curved catenary-ruled surfaces inexpensively.

Referring to Fig. 11(d), it can be seen that the catenary arches were stable without actuation strings, meaning they could stand under their self-weight (which were not collapsed or inclined). The stable behavior was attributed to three main factors. First, the arches were generated from inverse catenary rulings. Hence, they were naturally compression structures and could effectively perform the 'arch action', referring to the resistance mechanism against progressive collapse in large-span structures. Second, using the base with inclined abutments allowed the compression load to be effectively transferred to the supports in both horizontal and vertical directions. Specifically, the horizontal support reactions could prevent the arches from opening up further, thus stabilizing them. Finally, the proposed splitting algorithm led to arches possessing catenary rulings of similar sizes and shapes. Hence, the arches could perform similarly to inverse catenary curves without inclinations under their self-weight.

5. Discussion

Regarding the shape of the constructed surfaces, the proposed string actuation system has been validated for symmetric catenary-ruled surfaces. Catenary-ruled surfaces are asymmetric when their h or $\vec{G}$ are changed, as mentioned in Figs. 5(b) and (d). The arches split from the asymmetric surface may invalidate the self-correction mechanism in Section 4.2.1. Thus, the validation of the proposed system for asymmetric catenary-ruled surfaces will be our future work. For free-form surfaces, the main challenge of building them using the proposed string actuation system is the subdivision approach. The existing string actuation system requires that the divided local sub-structures, such as catenary arches, are stable under their self-weight. However, the sub-structures divided from a free-form surface might not be self-supporting. As a result, the sub-structures assembled by lifting may collapse when placed on the ground to form the target surface. Therefore, extending the proposed construction method to free-form surfaces requires further development.

For the proposed splitting method, performing inappropriate division on the catenary-ruled surface may lead to assembly failure. In detail, if the pre-defined division interval is too small, the shapes of the produced arches will become narrow, which means that their ability to resist external forces is decreased due to a significant reduction in the support area. This increases the risk of collapse during placement. On the contrary, a division interval that is too large may produce arches with excessive curvature change. In doing so, the load between adjacent arches may increase due to uneven weight distribution, leading to inclinations of arches or even assembly failure. The proposed splitting algorithm only gives a controllable method, but robustly finding a suitable division interval in general cases requires further research.

In terms of developing the string actuation system, this study explored other methods to put and remove the strings. For example, a potential idea is pulling the string on the ground to assemble arches. This can be achieved by putting the string inside the panels and letting the string thread out on one side of the arch. However, complex string tunnels can bring about additional design and fabrication costs, and the pulling process requires an additional blocker to limit the movement of panels to make all panels fit each other tightly. In contrast, the proposed method of putting the string outside can simplify the manufacture of panels to save fabrication costs, and vertical lifting can utilize the effect of gravity to close the gap, which avoids the use of the blocker and additional labor consumption. Moreover, as

mentioned in Section 3.3, the actuation strings may not need to be removed. Instead, they may be post-tensioned to enhance the structural performance of the arches. However, the strings were removed in this study for aesthetic reasons.

In the development of catenary-ruled surfaces, a detailed structural analysis is needed. This analysis, especially when considering each panel as a rigid body, is integral to comprehensively understanding the mechanical behavior and properties of these surfaces. While our current study lays the groundwork for the construction and design of these surfaces, we acknowledge the need for further research focused on structural analysis. Future studies will be aimed at exploring the intricate dynamics and mechanical responses of these surfaces under varied conditions, thereby providing a more holistic understanding of their potential applications and limitations.

This study only tested small-scale prototypes, which may present challenges when scaling up the result to larger-span structures. First, due to increased weight, the behavior of the actuated strings and their ability to maintain the desired form of the strips may differ in larger structures. The tensile strength, elasticity, and deformation of the strings could lead to deviations from the intended geometry. Second, assembling large-scale structures may result in the accumulation of errors, which could require manual adjustments to correct the alignment of discrete panels. Third, some environmental factors, such as wind loads and temperature variations, could cause additional stresses that are negligible in small-scale prototypes.

The large-scale construction of catenary-ruled surfaces has huge potential to be achieved by using existing techniques. The 3D-printed panels can be replaced with precast concrete panels. The rings on the top surface of the panels can be replaced with the commonly used ring screws. The lift and place process (see Figs. 11(a)–(c)) may be simply achieved using a crane to control the folding motion and placement locations of arches. The main challenges may be fine-tuning the locations of arches and removing the actuation strings (see Fig. 11(d)). Both tasks can be highly skill-demanding and may be time-consuming in large-scale constructions. Nevertheless, due to the use of the zig-zag interlock mechanism between arches, arranged arches can always form the approximate shape of the target catenary-ruled surface without fine-tuning. Hence, it can be understood that fine-tuning is only needed for applications where accuracy is critical. Besides, the actual construction may have higher requirements for structural performance. This can be solved by strengthening the connections between arches so that the surface can act as a whole to enhance the structural performance. The abovementioned concerns in large-scale applications will be closely studied in our future work, aiming to achieve a simple, accurate, and reliable construction method.

Moving forward, we plan to investigate the mechanical properties and structural performance of catenary-ruled surfaces at different scales. However, conducting a conceptual structural analysis, even on a small scale, is a challenging task. A large number of panels and their connections via cable ties can significantly increase the computational time and resources in structural analysis. Moreover, this complexity is compounded when considering the potential for different materials and construction methods in large-scale applications. Therefore, future research should focus on developing structural analysis methods that are tailored to these specific scenarios, ensuring that the findings are applicable and relevant to real-world, large-scale constructions of catenary-ruled surfaces.

6. Conclusion

This paper proposes a new geometry family of 'catenary-ruled surfaces', which uses catenary curves as rulings to create well-defined complex curved surfaces. The proposed modeling method is developed based on a combination of catenary curve design parameters and line-ruled surface definitions. Hence, this paper shows that the shape of catenary-ruled surfaces can be fully parameterized and systematically
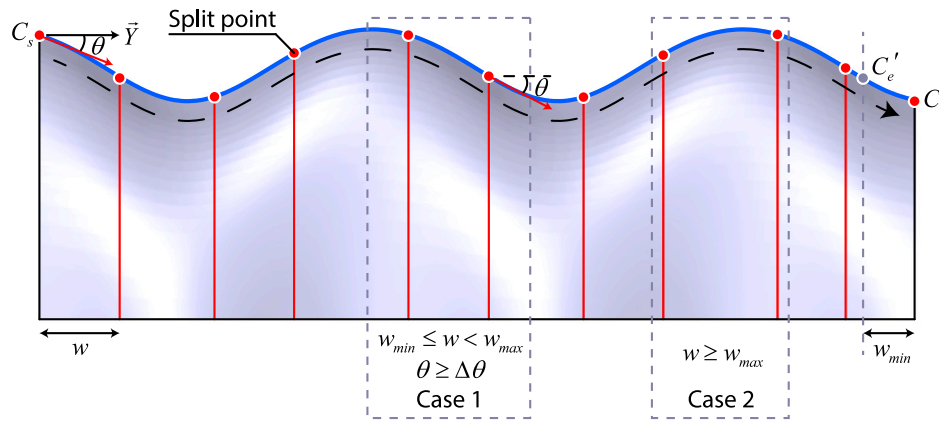
Fig. A.12. The right view of the tunnel example. The blue curve is the ridge, C, and the red points represent the split points. The dashed rectangles show the two cases to find split points. (For interpretation of the references to color in this figure legend, the reader is referred to the web version of this article.)

controlled using just four catenary curve design parameters. Varying these parameters provides new possibilities to simply, conveniently, and quickly create a wide variety of elegant architectural designs.

This paper also shows that a specific group of catenary-ruled surfaces, i.e., inverse catenary-ruled surfaces, can be effectively and inexpensively constructed by using the proposed string actuation system. This construction strategy is achieved using a series of catenary arches to form the prescribed catenary-ruled surface, where each arch is a mechanical mechanism made up of double-curved hexagonal panels connected by strings. It is demonstrated that controlling the movements of a single point on the actuation string determines the folding motion of the arch. More significantly, the proposed string actuation system has a self-correction mechanism due to the use of a closed-form actuation string so that the gaps between panels can be forced to close, thereby achieving the target catenary arch. Furthermore, this paper shows that the actuated arches are stable under their self-weight, as they are designed using inverse catenary rulings to act as an efficient structural system predominantly under pure compression. Finally, it is shown that using zig-zag boundaries between adjacent arches can effectively improve positioning accuracy when putting catenary arches together.

The limitations and future works of the proposed concepts are also discussed in this paper. We expect that the new modeling approach and construction strategy of double-curved surfaces will enable the development of a wide range of novel and efficient structures.

Declaration of competing interest

The authors declare that they have no known competing financial interests or personal relationships that could have appeared to influence the work reported in this paper.

Acknowledgments

Appendix A

The appendix introduces the details of the splitting algorithm. The algorithm requires five parameters: (1) the catenary-ruled surfaces, S, (2) the minimum width of arches, w_{min}; (3) the maximum width of arches, w_{max}; (4) an allowable angle difference, $\Delta\theta$ and (5) the number of the sampling points, N. Besides, the horizontal vector is set to be the global Y-axis, $\vec{Y}$, which is perpendicular to all the catenary

---

Algorithm 1: Splitting algorithm

    Input: S, $\Delta\theta$, N, w_{min} and w_{max}
    Output: S_p
1 $C \leftarrow$ Connect all peaks of the rulings on S;
2 S_p Add(C_s);
3 Find C'_e at a distance w_{min} from C_e;
4 $L \leftarrow$ Divide the curve from C_s to C'_e into N points;
5 **foreach** $p \in L$ **do**
6     $p' \leftarrow$ Find the previous split point of p;
7     $w \leftarrow$ Distance(p', p);
8   **if** $w_{cur} \geq w_{max}$ **then**
9       $p \leftarrow$ The point at a distance w_{max} from p';
10   S Add(p);
11   **else**
12      $\vec{V}_{cur} \leftarrow$ Tangent at p;
13      $\theta \leftarrow$ Vector angle ($\vec{Y}$, $\vec{V}_{cur}$);
14   **if** $\theta > \Delta\theta$ **then**
15   S_p Add(p);
16   **end**
17   **end**
18   S_p Add(C_e);
19    $Pl \leftarrow$ Get planes ($S_p, \vec{G}, \vec{Y}$);
20    $St \leftarrow$ Cut (Pl, S)
21 **end**

---

rulings. Note that w_{min} and w_{max} jointly determine the division interval mentioned in Section 5.

Fig. A.12 shows the right view of the tunnel. The splitting algorithm starts by connecting the peak of each catenary ruling to find the ridge (blue curve), C. Next, the algorithm finds the endpoint, C'_e, which is w_{min} away from the end of the ridge, C_e. It can ensure the last arch meets the width requirement. Then, the curve from the start point of the ridge, C_s, to C'_e can be divided into N sampling points, L. After that, a while loop is executed to search all potential split points from L. Each iteration checks if the current point, p, and the previous split point, p', can form a reasonable arch. In detail, the width of the arch, w, can be expressed by the horizontal distance from p to p'. The curvature variation of the strip is measured by the angle, θ, between the tangent of the current point and $\vec{Y}$. There are only two cases for creating reasonable split points: (1) if $w \geq w_{max}$, then the point that is w_{max} away from p' will be a split point, and (2) if $w_{min} \leq w < w_{max}$ and $\theta \geq \Delta\theta$, p will be signed as a split point. In this way, all split points, S_p, can be found efficiently, and each split point can form a cutting plane

(*Pl*) perpendicular to $\vec{Y}$. Finally, these planes cut the catenary-ruled surface to generate strips *St*. A pseudo-code of the splitting algorithm is shown in Algorithm 1.

Appendix B. Supplementary data

Supplementary material related to this article can be found online at https://doi.org/10.1016/j.istruc.2023.105755.

References

[1] Rippmann M, Mele TV, Popescu M, Augustynowicz E, Méndez Echenagucia T, Calvo Barentin CJ, et al. The armadillo vault: computational design and digital fabrication of a freeform stone shell. In: Adriaenssens S, Gramazio F, Kohler M, Menges A, Pauly M, editors. Advances in architectural geometry. Zurich; 2016, p. 344–63. http://dx.doi.org/10.3218/3778-4_23.

[2] Popescu M, Rippmann M, Liew A, Reiter L, Flatt RJ, Mele TV, et al. Structural design, digital fabrication and construction of the cable-net and knitted formwork of the knitcandela concrete shell. Structures 2021;31:1287–99. http://dx.doi.org/10.1016/j.istruc.2020.02.013.

[3] Bechert S, Groenewolt A, Krieg OD, Menges A, Knippers J. Structural performance of construction systems for segmented timber shell structures. In: Proceedings of the international association for shell and spatial structures symposium. 2018, p. 1–9.

[4] Fauche E, Adriaenssens S, Prevost JH. Structural optimization of a thin-shell bridge structure. J Int Assoc Shell Spat Struct 2010;51(164):153–60.

[5] Fenu L, Congiu E, Marano GC, Briseghella B. Shell-supported footbridges. Curved Layer Struct 2020;7(1):199–214. http://dx.doi.org/10.1515/cls-2020-0017.

[6] Liew A, Stürz YR, Guillaume S, Mele TV, Smith RS, Block P. Active control of a rod-net formwork system prototype. Autom Constr 2018;96:128–40. http://dx.doi.org/10.1016/j.autcon.2018.09.002.

[7] Ramm E. Shape finding of concrete shell roofs. J Int Assoc Shell Spat Struct 2004;45(144):29–39.

[8] Pottmann H, Asperl A, Hofer M, Kilian A. Architectural geometry. Bentley Institute Press; 2007.

[9] Adriaenssens S, Block P, Veenendaal D, Williams C. Shell structures for architecture: form finding and optimization. Routledge; 2014.

[10] Shelden D. Digital surface representation and the constructibility of Gehry's Architecture [Ph.D. thesis], Cambridge: Massachusets Institute of Technology.; 2002.

[11] Block P, Ochsendorf J. Thrust network analysis: a new methodology for three-dimensional equilibrium. J Int Assoc Shell Spat Struct 2007;48(155):167–73.

[12] Akbarzadeh M, Mele TV, Block P. On the equilibrium of funicular polyhedral frames and convex polyhedral force diagrams. Comput-Aided Des 2015;63:118–28. http://dx.doi.org/10.1016/j.cad.2015.01.006.

[13] Li Q, Su Y, Wu Y, Borgart A, Rots J. Form-finding of shell structures generated from physical models. J Int Assoc Shell Spat Struct 2017;32(1):11–33. http://dx.doi.org/10.1177/0266351117696577.

[14] Vouga E, Höbinger M, Wallner J, Pottmann H. Design of self-supporting surfaces. ACM Trans Graph 2012;31(4):1–11. http://dx.doi.org/10.1145/2185520.2185583.

[15] Liu Y, Pan H, Snyder J, Wang W, Guo B. Computing self-supporting surfaces by regular triangulation. ACM Trans Graph 2013;32(4):1–10. https://dl.acm.org/doi/10.1145/2461912.2461927.

[16] De Goes F, Alliez P, Owhadi H, Desbrun M. On the equilibrium of simplicial masonry structures. ACM Trans Graph 2013;32(4):1–10. http://dx.doi.org/10.1145/2461912.2461932.

[17] Meng X, Lee TU, Xiong Y, Huang X, Xie YM. Optimizing support locations in the roof–column structural system. Appl Sci 2021;11(6). http://dx.doi.org/10.3390/app11062775.

[18] Meng X, Xiong Y, Xie YM, Sun Y, Zhao ZL. Shape–thickness–topology coupled optimization of free-form shells. Autom Constr 2022;142:104476. http://dx.doi.org/10.1016/j.autcon.2022.104476.

[19] Panozzo D, Block P, Sorkine-Hornung O. Designing unreinforced masonry models. ACM Trans Graph 2013;32(4):1–12. http://dx.doi.org/10.1145/2461912.2461958.

[20] Deuss M, Panozzo D, Whiting E, Liu Y, Block P, Sorkine-Hornung O, et al. Assembling self-supporting structures. ACM Trans Graph 2014;33(6):1–10. http://dx.doi.org/10.1145/2661229.2661266.

[21] Veenendaal D, Block P. Design process for prototype concrete shells using a hybrid cable-net and fabric formwork. Eng Struct 2014;75:39–50. http://dx.doi.org/10.1016/j.engstruct.2014.05.036.

[22] Mele TV, Mehrotra A, Méndez Echenagucia T, Frick U, Augustynowicz E, Ochsendorf J, et al. Form finding and structural analysis of a freeform stone vault. In: Proceedings of the International Association for Shell and Spatial Structures (IASS) Symposium. 2016, p. 1–10.

[23] Kühnel W. Differentialgeometrie. Springer; 1999.

[24] Peternell M, Pottmann H, Ravani B. On the computational geometry of ruled surfaces. Comput-Aided Des 1999;31(1):17–32. http://dx.doi.org/10.1016/S0010-4485(98)00077-3.

[25] Prousalidou E, Hanna S. A parametric representation of ruled surfaces. In: Dong A, Moere AV, Gero JS, editors. Computer-aided architectural design futures (caadfutures) 2007. Springer; 2007, p. 265–78. http://dx.doi.org/10.1007/978-1-4020-6528-6_20.

[26] Mamieva IA. Influence of the geometrical researches of ruled surfaces on design of unique structures. Struct Mech Eng Constr Build 2019;15:299–307. http://dx.doi.org/10.22363/1815-5235-2019-15-4-299-307.

[27] Lee TU, Xie YM. From ruled surfaces to elastica-ruled surfaces: new possibilities for creating architectural forms. J Int Assoc Shell Spat Struct 2021;62(4):271–81. http://dx.doi.org/10.20898/j.iass.2021.014.

[28] Lee TU, You Z, Gattas JM. Elastica surface generation of curved-crease origami. Int J Solids Struct 2018;136:13–27. http://dx.doi.org/10.1016/j.ijsolstr.2017.11.029.

[29] Lee TU, Gattas JM, Xie YM. Bending-active kirigami. Int J Solids Struct 2022;254–255:111864. http://dx.doi.org/10.1016/j.ijsolstr.2022.111864.

[30] Bi M, He Y, Li Z, Lee TU, Xie YM. Design and construction of kinetic structures based on elastica strips. Autom Constr 2023;146:104659. http://dx.doi.org/10.1016/j.autcon.2022.104659.

[31] Lockwood EH. A book of curves. Cambridge University Press; 1961.

[32] Costa RS, Lavall ACC, da Silva RGL, dos Santos AP, Viana HF. Cable structures: an exact geometric analysis using catenary curve and considering the material nonlinearity and temperature effect. Eng Struct 2022;253:113738. http://dx.doi.org/10.1016/j.engstruct.2021.113738.

[33] Hart G, Heathfield E. Catenary arch constructions. In: Proceedings of bridges 2018: mathematics, art, music, architecture, education, culture. 2018, p. 325–32.

[34] Nikolić D. Catenary arch of finite thickness as the optimal arch shape. Struct Multidisc Optim 2019;60:1957–66. http://dx.doi.org/10.1007/s00158-019-02304-9.

[35] Kaplan G. The catenary: art, architecture, history, and mathematics. In: Bridges Leeuwarden: mathematics, music, art, architecture, culture. 2008, p. 47–54.

[36] Gohnert M, Bulovic L, Bradley R. A low-cost housing solution: earth block catenary vaults. Structures 2018;15:270–8. http://dx.doi.org/10.1016/j.istruc.2018.07.008.

[37] Huerta S. Structural design in the work of Gaudí. Archit Sci Rev 2006;49(4):324–39.

[38] Makert R, Alves G. Between designer and design: parametric design and prototyping considerations on gaudí's sagrada familia. Per Pol Arch 2016;47(2):89–93.

[39] Zhao Z, Zhang T, Wang W. A form-finding method for spatial arch bridges based on inverse hanging method. Structures 2022;46:64–72. http://dx.doi.org/10.1016/j.istruc.2022.10.058.

[40] Tepavčević B, Stojaković V, Mitov D, Bajšanski I, Jovanović M. Design to fabrication method of thin shell structures based on a friction-fit connection system. Autom Constr 2017;84:207–13. http://dx.doi.org/10.1016/j.autcon.2017.09.003.

[41] Wang Z, Song P, Isvoranu F, Pauly M. Design and structural optimization of topological interlocking assemblies. ACM Trans Graph 2019;38(6):1–13. http://dx.doi.org/10.1145/3355089.3356489.

[42] Ma L, He Y, Sun Q, Zhou Y, Zhang C, Wang W. Constructing 3D self-supporting surfaces with isotropic stress using 4D minimal hypersurfaces of revolution. ACM Trans Graph 2019;38(5):1–13. https://dl.acm.org/doi/10.1145/3188735.

[43] Kilian M, Monszpart A, Mitra NJ. String actuated curved folded surfaces. ACM Trans Graph 2017;36(3):1–13. http://dx.doi.org/10.1145/3072959.3015460.

[44] Plasencia Alava KB, McCann LK, Hodge G, Baber K, Gattas JM. Computational design and experimental behaviour of deployable mass timber arches. J Int Assoc Shell Spat Struct 2019;60(1):90–100. http://dx.doi.org/10.20898/j.iass.2019.199.030.

[45] Long A, Kirkpatrick J, Gupta A, Nanukuttan S, Polin DM. Rapid construction of arch bridges using the innovative flexiarch. In: Proceedings of the institution of civil engineers - bridge engineering. 2013, p. 143–53. http://dx.doi.org/10.1680/bren.11.00036.

[46] Long A, Gupta A, Mcpolin DO, Cook J. Adapting the Flexiarch for widening a complex arch bridge. In: Proceedings of the institution of civil engineers - bridge engineering. 2018, p. 246–51. http://dx.doi.org/10.1680/jbren.17.00007.

[47] Happold E, Liddell WI. Timber lattice roof for the Mannheim Bundesgartenschau. Struct Engr 1975;53(3):99–135.

[48] Panetta J, Konaković-Luković M, Isvoranu F, Bouleau E, Pauly M. X-shells: a new class of deployable beam structures. ACM Trans Graph 2019;38(4):1–15. http://dx.doi.org/10.1145/3306346.3323040.

[49] Baverel O, Caron JF, Tayeb F, Du Peloux L. Gridshells in composite materials: construction of a 300 m^2 forum for the solidays' festival in Paris. Struct Eng Int 2012;22(3):408–14. http://dx.doi.org/10.2749/101686612X13363869853572.

[50] Tayeb F, Caron JF, Baverel O, Du Peloux L. Stability and robustness of a 300 m^2 composite gridshell structure. Constr Build Mater 2013;49:926–38. http://dx.doi.org/10.1016/j.conbuildmat.2013.04.036.

[51] Carlson SC. Catenary, encyclopedia britannica. 2017, https://www.britannica.com/science/catenary. (Accessed 21 July 2022).

[52] Vasek J, Suchard O. Numerical analysis of gravity and parabolic catenaries. Math Models Methods Appl Sci 2014;8:156–64. http://dx.doi.org/10.1016/j.engstruct.2021.113738.

[53] Salomon D. Curves and surfaces for computer graphics. Springer New York; 2006.

[54] Kilian A. Linking digital hanging chain models to fabrication. In: Proceedings of the 23rd Annual Conference of the Association for Computer Aided Design in Architecture and the 2004 Conference of the AIA Technology in Architectural Practice Knowledge Community. 2004, p. 110–25. http://dx.doi.org/10.52842/conf.acadia.2004.110.

[55] Floater MS, Hormann K. Surface parameterization: a tutorial and survey. In: Dodgson NA, Floater MS, Sabin MA, editors. Advances in multiresolution for geometric modelling. Berlin: Springer; 2005, p. 157–86. http://dx.doi.org/10.1007/3-540-26808-1_9.

[56] Gu X, Yau ST. Global conformal surface parameterization. In: Kobbelt L, Schroeder P, Hoppe H, editors. Proceedings of the 2003 Eurographics/ACM SIGGRAPH Symposium on Geometry Processing. 2003, p. 127–37. http://dx.doi.org/10.2312/SGP/SGP03/127-137.

[57] Botsch M, Kobbelt L, Pauly M, Alliez P, Lévy B. Polygon mesh processing. CRC Press; 2010.

[58] Allen E, Zalewski W. Form and forces: Designing efficient, expressive structures. John Wiley and Sons; 2010.